ELSEVIER

Marine Chemistry 76 (2001) 271–283

MARINE CHEMISTRY

www.elsevier.com/locate/marchem

Quantum yield for the photochemical production of dissolved inorganic carbon in seawater

Sophia C. Johannessen [a,b,*], William L. Miller [a]

[a] Department of Oceanography, Dalhousie University, Halifax, Nova Scotia, Canada, B3H 1P2
[b] Institute of Ocean Sciences, Contaminant Chemistry, 9860 W. Saanich Rd. North Saanich, B.C. Canada V8L 4B2

Received 4 April 2001; received in revised form 16 July 2001; accepted 10 August 2001

Abstract

The direct photooxidation of coloured dissolved organic matter (CDOM) to dissolved inorganic carbon (DIC) may provide a significant sink for organic carbon in the ocean. To calculate the rate of this reaction on a global scale, it is essential to know its quantum yield, or photochemical efficiency. We have determined quantum yield spectra, $\phi(\lambda)$, (moles DIC/mole photons absorbed) for 14 samples of seawater from environments ranging from a turbid, eutrophic bay to the Gulf Stream. The spectra vary among locations, but can be represented quite well by three pooled spectra for zones defined by location and salinity: inshore $\phi(\lambda) = e^{-(6.66+0.0285(\lambda-290))}$; coastal $\phi(\lambda) = e^{-(6.36+0.0140(\lambda-290))}$; and open ocean $\phi(\lambda) = e^{-(5.53+0.00914(\lambda-290))}$. Production efficiency increases offshore, which suggests that the most highly absorbing and quickly faded terrestrial chromophores are not those directly responsible for DIC photoproduction. © 2001 Elsevier Science B.V. All rights reserved.

Keywords: Marine photochemistry; Carbon cycle; Quantum yield; Coloured dissolved organic matter; Organic carbon; Carbon dioxide

1. Introduction

The photochemical oxidation of coloured (or chromophoric) dissolved organic matter, CDOM, is important for carbon cycling in the ocean. Photochemical oxidation in the coastal zone may provide the unknown sink for terrestrial dissolved organic carbon, DOC (Kieber and Mopper, 1987; Kieber et al., 1989, 1990; Mopper et al., 1991; Valentine and Zepp, 1993; Miller, 1994; Moran and Zepp, 1997; Vodacek et al., 1997; Johannessen, 2000). In the open ocean, it provides a hitherto unquantified, but possibly important, sink for DOC produced in situ (Mopper et al., 1991). Biologically and chemically reactive photoproducts can participate in secondary transformations of organic carbon. Biologically labile photoproducts include ammonium and amino acids (Bushaw et al., 1996), and low molecular weight organic compounds (Kieber et al., 1989, 1990; Wetzel et al., 1995; Ratte et al., 1998; and review by Moran and Zepp, 1997). Hydroxyl radical (Mopper and Zhou, 1990; Zhou and Mopper, 1990; Zepp et al., 1992), oxygen radicals (review by Blough and Zepp, 1995), total free radicals (Zafiriou and Dister, 1991), hydrogen peroxide (Moore et al., 1993; Sikorski and Zika, 1993; Miller and Kester, 1994a),

---

[*] Corresponding author. Department of Oceanography, Dalhousie University, Halifax, Nova Scotia, Canada, B3H 1P2. Tel.: +1-250-363-6616; fax: +1-250-363-6310.

E-mail address: johannessen@pac.dfo-mpo.gc.ca (S.C. Johannessen).

PII: S0304-4203(01)00067-6

reduced iron (Finden et al., 1984; Miller and Kester, 1994b), and COS (Andreae and Ferek, 1992) are among the chemically reactive species formed.

CDOM can also be photomineralized directly into various inorganic carbon gases. Mopper et al. (1991) reported that carbon monoxide was by far the most rapidly produced carbon photoproduct they were able to measure in seawater. However, Miller and Zepp (1995) found that dissolved inorganic carbon, DIC (measured as the sum of CO_2, HCO_3^-, and CO_3^{-2}) was produced from CDOM about 20 times as fast as CO in the near coastal water of the Mississippi River plume. Further comparison by Miller and Moran (1997) found DIC production to be 15 times as fast as CO production for coastal marsh water. The direct photoproduction of DIC from CDOM represents a mineralization pathway that does not require microbial oxidation. Vähätalo et al. (2000a) determined spectral quantum yield or efficiency for DIC production in situ in a Scandinavian lake, using tubes suspended at several depths. Gao and Zepp (1998) have recently published quantum yield values at three wavelengths for a sample of water from the Satilla River, GA, USA, and Moore (1999) determined the spectral quantum yield for DIC photoproduction in Nova Scotian lake water. To date, there have been no published DIC quantum yield spectra for seawater.

Without quantum yield spectra, it is impossible to estimate quantitatively the regional or global photochemical production rate of DIC as a sink for DOC. Here, we present DIC quantum yield spectra for seawater from the Gulf Stream, the Mid-Atlantic Bight, and Halifax Harbour, Nova Scotia. We also describe the variability of DIC quantum yield with location and depth, and suggest an explanation for that variability.

2. Methods

2.1. General approach

The quantum yield of a primary photochemical reaction at a particular wavelength is defined as the ratio of the number of moles of reactant consumed or of product made (Braslavsky et al., 1996), in this case DIC, to the number of moles of photons absorbed at that wavelength. (Table 1 contains a summary of the symbols and abbreviations used in this paper.) Because neither the molar absorptivity of the chromophore nor the reaction mechanism responsible for the photochemical production of DIC is known, we actually calculate a wavelength-dependent "apparent" quantum yield, $\phi(\lambda)$, as shown in Eq. (1):

$$\phi(\lambda) = \frac{\text{moles of DIC produced}}{\text{moles of photons absorbed by CDOM}(\lambda)}. \tag{1}$$

The production rate of DIC, dP/dt (moles DIC produced m^{-3} s^{-1}), in an optically thin solution can be expressed as:

$$dP/dt = \int \left(E_0(\lambda) a_{\mathrm{CDOM}}(\lambda) \phi(\lambda) d\lambda \right), \tag{2}$$

(modified from Balzani and Carassiti, 1970), where $E_0(\lambda)$ is the scalar irradiance (moles photons m^{-2} s^{-1} nm^{-1}), $a_{\mathrm{CDOM}}(\lambda)$ is CDOM absorptivity (m^{-1}), and λ is wavelength (nm). By measuring the spectral

Table 1
Sample names and locations

Sample name	Latitude (°N)	Longitude (°W)
M9705-03s	38.67	74.88
M9705-03d	38.67	74.88
M9705-05s	30.52	74.68
M9705-05d	30.52	74.68
M9705-16s	36.21	72.00
M9708-08s	37.27	74.36
M9708-08d	37.27	74.36
M9708-16As	36.21	72.00
M9708-16Ad	36.21	72.00
F9805-01	44.73	63.66
F9805-03	44.71	63.67
F9805-04	44.70	63.66
NW Arm 9906 (unfaded)	44.62	63.56
NW Arm 9906 (faded)	44.62	63.56

Samples beginning with "M" come from the Mid-Atlantic Bight; those beginning with "F" come from the Bedford Basin of Halifax Harbour; and "NW Arm" refers to the North West Arm of Halifax Harbour. The four digits following the location code refer to the year and month of collection, e.g. "9708" means August 1997. The number following the hyphen is the station number, and "s" and "d" mean surface and deep, i.e. below the mixed layer, respectively.

irradiance, spectral absorptivity, and production rate as described below, we can calculate the spectral quantum yield for DIC production. (In the solar simulator, we measured downwelling irradiance, not scalar irradiance, but since the cells were arranged on a black velvet cloth inside the irradiation box and the incident radiation was approximately collimated, the measurement was reasonable.)

2.2. Sample collection and storage

Samples were taken from the Gulf Stream, the Mid-Atlantic Bight, and Halifax Harbour, Nova Scotia. Table 2 contains a list of sample names and locations. We collected 1 l of seawater from the surface and 1 l from below the mixed layer at each station, using Niskin bottles, except in Halifax Harbour, where we only collected water from the surface. Water samples were filtered within a day of collection through 0.2 μm Schleicher and Schuell Nylon 66 filters to remove particles and bacteria. The Halifax Harbour samples and those taken during the August 1997 cruise in the Mid-Atlantic Bight were pressure-filtered using a peristaltic pump with an in-line filter; the others were vacuum-filtered. After filtration, samples were stored at 4 °C in amber glass bottles for less than a year to minimize biological activity and photochemical breakdown of CDOM. The absorbance spectra of the samples did not change appreciably over the storage time. (Related studies have shown no measurable change in absorbance at 350 nm over three months of storage under the same conditions.)

Table 2
Symbols and abbreviations used in the text (following Braslavsky et al., 1996, where applicable)

$A_{\mathrm{CDOM}}(\lambda)$	Absorbance by CDOM (AU)
$a_{\mathrm{CDOM}}(\lambda)$	Absorptivity by CDOM (m^{-1})
C	Constant in absorptivity correction equation (dimensionless)
CDOM	Coloured dissolved organic matter
DIC	Dissolved inorganic carbon
DOC	Dissolved organic carbon
$E_{\mathrm{d}}(\lambda)$	Incident (downwelling) irradiance (moles photons $\mathrm{m}^{-2}\ \mathrm{s}^{-1}\ \mathrm{nm}^{-1}$)
$\phi(\lambda)$	Apparent quantum yield (moles DIC produced/mole photons absorbed)
λ	Wavelength (nm)
m_1	Regression constant in quantum yield fitting equation
m_2	Regression constant in quantum yield fitting equation
$\mathrm{d}P/\mathrm{d}t$	Production rate of DIC (moles DIC $\mathrm{m}^{-3}\ \mathrm{s}^{-1}$)
S	Absorptivity slope from fitting equation (nm^{-1})
UV	Ultraviolet radiation
UVA	Radiation from 320 to 400 nm
UVB	Radiation from 280 to 320 nm
z	Path length of spectrophotometer cell or depth in the ocean (m)

2.3. DIC stripping and irradiations

All carbonate species initially present were stripped from samples prior to irradiation, in order to measure the low concentrations of DIC produced photochemically. Each stored sample was refiltered sequentially through two 0.2 μm Schleicher and Schuell Nylon 66 filters into an acid-washed, distilled water-rinsed, glass Erlenmeyer flask and then into a similarly cleaned glass sparging vessel. After acidification to a pH between 3 and 4 with concentrated HCl, CO_2-free air was bubbled through the sample until no measurable DIC remained (< 0.3 μM). The stripped seawater was buffered back to approximately the original pH (initial pH ranged from 7.8 to 8.3) with powdered Fisher ACS sodium borate ($Na_2B_4O_7 \cdot 10H_2O$). The addition of the acid and the buffer to a sample was found to increase its UVB absorptivity by about 5%, leaving the longer-wavelength portion of the spectrum essentially unchanged. Control experiments showed that neither the added reagents nor the filtration process produced measurable DIC photochemically. It was not feasible to strip the DIC from seawater samples without acidification; without acidification, even after 2 days of bubbling with CO_2-free air, we measured no significant decrease in the DIC concentration. Although it is possible that the changes in pH during the DIC stripping changed the photochemical reactivity of the DOC, it is unlikely that any such change was significant: Miller and Zepp (1995) found only a 15% increase in DIC photoproduction under full spectral irradiance in samples that were irradiated at a pH of 3.5 relative to those samples which had been rebuffered to approximately their original pH. In addition, the lake DIC quantum yield spectrum (Moore, 1999) shown in Fig. 10 was obtained without initial stripping of DIC (because fresh water has a much lower concentration of DIC than does the ocean), and it is similar to those determined in this study.

Quartz irradiation cells and their silicon fittings were sterilized for at least 3 h under a Phillips TUV 30W/G30 T8 long-life ultraviolet UV-C source in a laminar flow clean hood before each experiment. The fittings were attached to the irradiation cells inside the laminar flow hood. The DIC-free seawater was injected into the irradiation cells through their silicon septa directly from the sparger's sample port, using a new, sterile, hypodermic needle for each experiment. We wore gloves whenever handling the glassware. The acid-washing, sterilization, double 0.2 μm filtration and use of gloves proved to be essential for avoiding bacterial contamination of the irradiated samples, which otherwise resulted in increased CO_2 production due to respiration in the dark cells and under the longer wavelength cut-off filters.

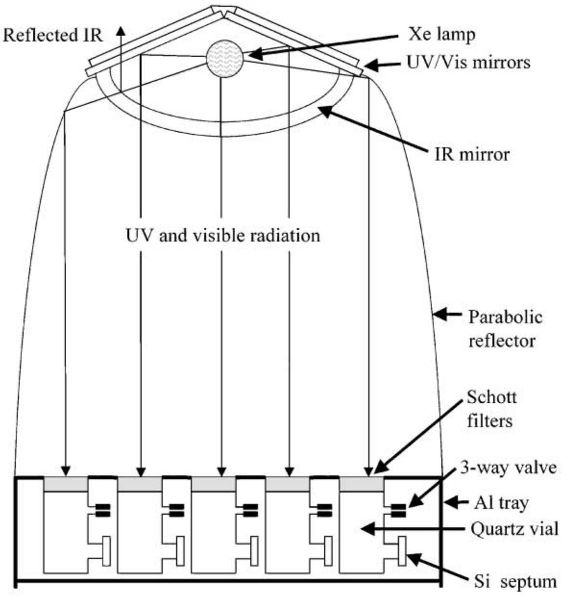

Fig. 1. Solar simulator with irradiation cells (modified from Moore, 1999).

Samples were irradiated in a Suntest CPS solar simulator with a 1000-W Heraeus xenon lamp fitted with an infrared mirror to lessen sample chamber heating. Samples maintained a temperature of approximately 27 °C during irradiations. Fourteen quartz irradiation cells were arranged in an aluminum and brass frame under Schott long-pass cut-off filters as shown in Fig. 1. Each cell was wrapped in black electrical tape, leaving only the ends open, to prevent the lateral leakage of radiation between cells. Two dark cells were included in each irradiation to correct for nonphotochemical production of DIC. Cells were always oriented as nearly vertical as possible (within 5° of vertical) to avoid path length variations. The method was not very sensitive to such variations, however, since one cell with a 30° tilt away from vertical showed only 10% less DIC production than observed in previous irradiations.

The spectral irradiance measured under each filter is shown in Fig. 2. The filters transmitted about 90% of incident radiation at long wavelengths, cutting off short-wavelength radiation, and had 50% transmission at one of the following "cut-off" wavelengths: 280, 295, 320, 335, 380, and 480 nm. Six pairs of matched filters were used for replicate irradiations. It was not always possible to obtain data from replicate samples because of limited sample volumes and because some samples developed bubbles during irradiation, making them unusable. Where replicates were used, the two production values were usually within 5% of one another. Irradiation times varied from 4 to 7 h. Spectral irradiance was measured under each filter with an Optronics OL754 spectroradiometer fitted with a fibreoptic cable. The spectroradiometer, with fibreoptic cable in place, was calibrated with an Optronics OL752-10E irradiance standard. Successive measurements with the spectroradiometer showed less than 1% variation in the irradiance measured at any wavelength.

To test the effect of irradiation history on quantum yield, we irradiated 1 l of water from the North West Arm of Halifax Harbour in an open borosilicate container for 111 h at the full output intensity of the solar simulator prior to other experimentation. UV-transparent polyethylene film was used to prevent evaporation during the experiment. We then conducted two quantum yield experiments as usual, one on the prefaded water and the other on a portion of the same sample which had not been previously faded.

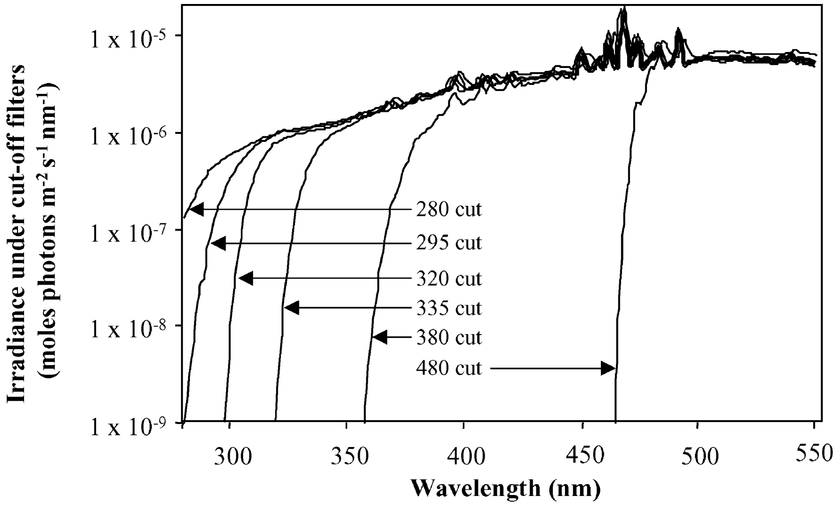

Fig. 2. Irradiance measured under cut-off filters.

2.4. DIC measurements

After irradiation, several milliliters of water from each irradiation cell were extracted with a hypodermic needle into a 10 ml gas-tight syringe though the silicon septum. Three to seven replicate 200 μl subsamples were injected into an acid trap and sparger for introduction into the CO_2 analyzer system. The phosphoric acid (pH = 2) in the acid trap converted the DIC into CO_2 following injection, and the resulting CO_2 was stripped from the sample and carried into the system in a stream of UHP (Ultra High Purity grade) nitrogen gas. The sample CO_2 passed sequentially through Drierite (anhydrous $CaSO_4$, Hammond Drierite) and magnesium perchlorate ($Mg(ClO_4)_2$, Aldrich ACS) columns to remove water vapor before entering a Li–Cor 6262 CO_2/H_2O infrared detector. The CO_2 analyzer was calibrated daily with a series of standards (0, 5, 10 and 20 μM DIC) made each day from a stock 5 mM sodium carbonate solution that was made freshly about once a month from dried sodium carbonate (Na_2CO_3, BDH AnalaR) and stored in an air-tight flask. The standards were injected into the acid trap and flowed through the system in exactly the same way as the samples. Calibration curves always resulted in $r^2 \geq 0.97$. The standard deviation of the mean of 50 replicate injections of distilled water was 0.16 μM. The limit of detection, defined as three times the standard deviation for the distilled water measurement, was 0.5 μM. This is definitely a conservative estimate of precision, since the distilled water injections were done over several months and their standard deviation included the day-to-day variability of the machine, while a new standard curve was made every day. Since the dark DIC production was typically the same as that measured under the 480 nm cut-off filter (< 0.3 μM over the 4–7-h irradiations), we used the 480 nm cut-off DIC production as a dark correction. The quantum yield spectra were determined using the corrected DIC production rates.

2.5. Absorbance measurements

We measured the spectral absorbance of each filtered, DIC-stripped, unirradiated sample with reagents added, so that it represented as closely as possible the colour of the solution that was irradiated. Spectral absorbance was measured in a 10 cm quartz cell with a Varian CARY3 scanning spectrophotometer. Absorbance, $A_{CDOM}(\lambda)$ (AU) was measured over the range 280–800 nm, and the values were converted to absorptivity, $a_{CDOM}(\lambda)$ (m^{-1}), according to the relation:

$$a_{CDOM}(\lambda) = 2.303 A_{CDOM}(\lambda)/z, \quad (3)$$

where z is the path length of the spectrophotometer cell in meters, and the factor 2.303 converts from log base ten to natural log (Braslavsky et al., 1996). We made a correction for scattering, index of refraction and blank drift by fitting Eq. (4) to the data. The use of an equation of this form to fit CDOM absorbance data has been described by Markager and Vincent (2000); Stedmon et al. (2000) and Johannessen (2000). Because of the difficulty of measuring a_{CDOM} at long wavelengths, particularly, in the open ocean samples, the fit was determined over the range 280–550 nm:

$$a_{\mathrm{CDOM}}(\lambda) = C\mathrm{e}^{-S\lambda} + a_0, \tag{4}$$

where C (m^{-1}), S (nm^{-1}) and a_0 (m^{-1}) are constants and λ is wavelength (nm). The offset, a_0, was then subtracted from the whole spectrum. The fit was not used for any purpose other than to provide an offset value. The corrected absorbance measured at each wavelength was used in subsequent calculations. Fig. 3 shows the absorptivity spectra for the darkest and clearest samples. For clarity, only two spectra are shown.

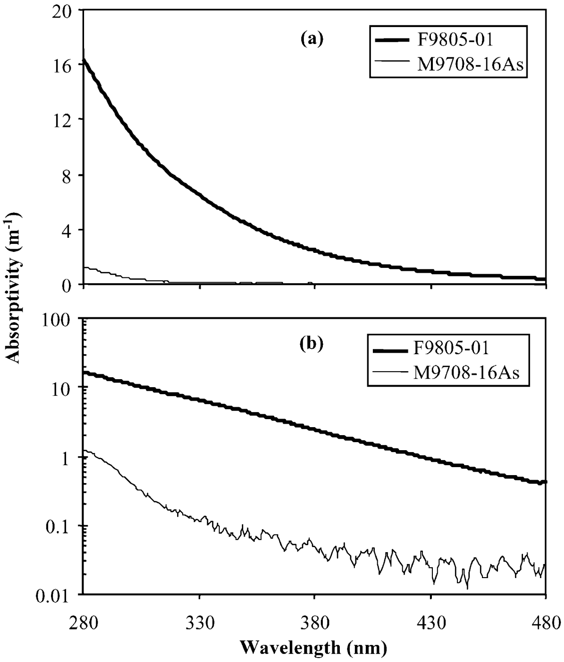

Fig. 3. Absorptivity spectra for the darkest (F9805-01) and clearest (M9708-16As) stations used in this study. For graphical clarity, only two spectra are shown.

2.6. Determination of quantum yield spectra

Quantum yield is sometimes calculated at discrete wavelengths by difference. The difference method consists of dividing the difference between the number of moles of DIC produced under filters with adjacent wavelength cut-offs by the difference between the irradiance measured under the two filters, as described by Xie et al. (1998). For example:

$$\phi(287.5\,\mathrm{nm}) = \frac{\dfrac{\mathrm{d[DIC]}}{\mathrm{d}t}(280\,\mathrm{cut}) - \dfrac{\mathrm{d[DIC]}}{\mathrm{d}t}(295\,\mathrm{cut})}{E_0(280\,\mathrm{cut})\,a_{\mathrm{CDOM}} - E_0(295\,\mathrm{cut})\,a_{\mathrm{CDOM}}}. \tag{5}$$

The resulting quantum yield point is then plotted at the wavelength halfway between the two successive cut-off filters.

We used the difference method described above as an order-of-magnitude and spectral shape check. However, this method was complicated by the nonuniformity of the irradiance field in the solar simulator, which required a normalization of all the production and irradiance values. The difference method is also quite sensitive to individual outlying production values. And plotting the quantum yield at the midpoint between the two cut-off wavelengths is not ideal where quantum yield changes rapidly with wavelength; the point should actually be plotted closer to the shorter cut-off wavelength, as explained by Rundel (1983) and Cullen and Neale (1994).

Because of these major disadvantages to the difference method, we chose to use a statistical curve fit method modified from those presented by Rundel (1983) and by Cullen and Neale (1994). The curve fit method assumed a spectral shape for quantum yield and required input data for the measured spectral irradiance and DIC production values for each cell under the long-pass filters. A Matlab® program then calculated best fit parameters, m_1 and m_2, for the equation:

$$\phi(\lambda) = \mathrm{e}^{-(m_1 + m_2(\lambda - 290))}, \tag{6}$$

where $\phi(\lambda)$ is apparent quantum yield (moles DIC produced/mole photons absorbed), and λ is wavelength (nm), over the range 280–550 nm at 1-nm intervals. This wavelength range was chosen because the absorbance data were unreliable at wavelengths longer than 550 nm; since there was no measurable DIC photoproduction under the 480 nm cut-off filter, the limited wavelength range should not have biased the results. The program changed the fitting parameters, m_1 and m_2, iteratively from initial estimates to find the best match between the measured production values and those predicted by Eq. (2) using the actual absorbance and irradiance spectra for each cell. (Initial evaluation of DIC production under successive cut-off filters indicated an exponential shape to the quantum yield spectra. We also tried to fit the production values with several other functional forms, including a linear fit and a double exponential. None of these forms fit as well as the single exponential for all samples, and it seemed an unwarranted interpretation of the data to choose a more complicated equation.)

3. Results

We determined the apparent spectral quantum yield for each of 14 samples from the Gulf Stream, the Mid-Atlantic Bight, and the Northwest Arm and Bedford Basin of Halifax Harbour, Nova Scotia (Johannessen, 2000). Taken together, the spectra were quite variable, both in shape and in magnitude. Table 3 contains a summary of the quantum yield equations.

The agreement between measured DIC production values for each cell and those predicted from the quantum yield spectra was very good, with r^2 values ranging from 0.92 to 0.99. Fig. 4 shows plots of predicted vs. measured DIC production values for the best and worst fits obtained from the 14 exposures. (Panel (b) of Fig. 4 shows only five points; we had to reject the data from both replicates under one filter in that experiment, because the cells had leaked. That panel shows the worst case used in these calculations.) Fig. 4 demonstrates that even the worst fit described the observed production rates reasonably well. Eleven of the fourteen calculated quantum yield spectra predicted DIC production with $r^2 > 0.96$. Error bars in Fig. 4 show the 95% confidence intervals for measured DIC production, determined from replicate distilled water injections, as described in the Methods section.

Table 3
Apparent quantum yield fit parameters (with standard deviations) for the equation $\phi = e^{-(m_1 + m_2(\lambda - 290)}$

Sample name	m_1 (S.D.)	m_2 (S.D.)
Inshore samples		
NW Arm 9906 (unfaded)	7.5 (0.8)	0.0096 (0.01)
M9708-08s	6.0 (0.5)	0.041 (0.009)
F9805-01	6.7 (0.9)	0.026 (0.02)
F9805-03	5.9 (0.8)	0.051 (0.03)
F9805-04	7.0 (0.3)	0.032 (0.01)
Inshore pooled spectrum	6.66 (1)	0.0285 (0.03)
Coastal samples		
M9708-08d	6.2 (0.5)	0.013 (0.01)
M9705-05s	6.1 (0.5)	0.020 (0.01)
M9705-05d	7.1 (1)	0.0083 (0.008)
NW Arm 9906 (faded)	5.7 (0.4)	0.017 (0.007)
Coastal pooled spectrum	6.36 (1)	0.0140 (0.02)
Open ocean samples		
M9705-16s	5 (2)	0.012 (0.01)
M9708-16As	5.3 (0.3)	0.013 (0.004)
M9708-16Ad	5.7 (0.6)	0.0073 (0.007)
Open ocean pooled spectrum	5.53 (0.7)	0.00914 (0.008)
Stn 3 (should be inshore)		
M9705-03s	3.6 (0.9)	0.058 (0.03)
M9705-03d	5.9 (1)	0.0068 (0.007)

Pooled spectra calculated as best fit to all production and irradiance data for each zone. These spectra should not be applied for wavelengths longer than 480 nm, since the efficiency of the reaction is effectively zero beyond that wavelength.

Because some readers may be more accustomed to seeing discrete results, such as those produced by the difference method, we have compared the results of the two methods for one quantum yield spectrum in Fig. 5. Fig. 5 demonstrates that the assumption of a single exponential shape to the quantum yield spectrum is not unreasonable. The two spectra diverge only at the shortest wavelength where, because of the small difference in incident irradiance between successive cut-off filters, the difference method is unreliable.

In general, the offshore quantum yield spectra were shallower than the inshore ones, and their magnitude at 300 nm was greater. To evaluate the combined effects of the trends in quantum yield slope and magnitude independently of variations in

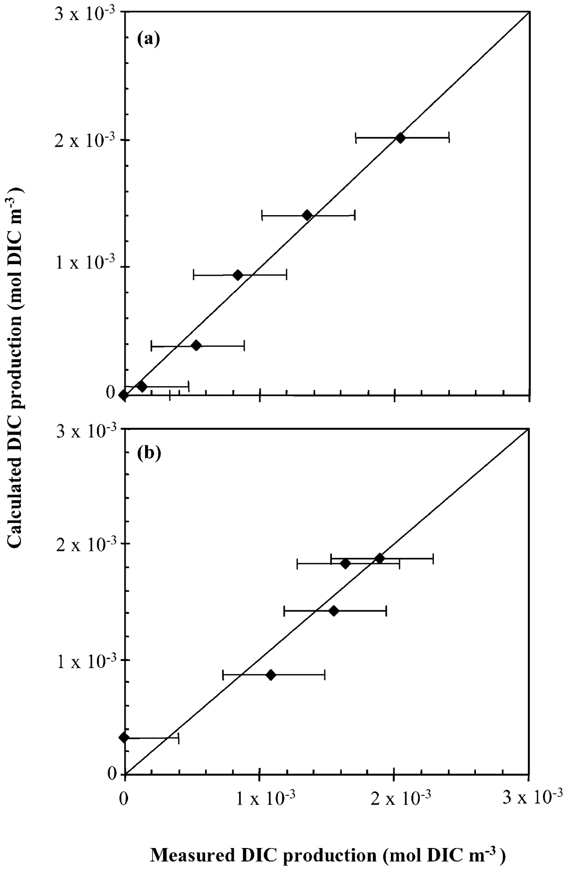

Fig. 4. Predicted vs. measured DIC photoproduction in irradiation cells for samples with the best and worst fits: (a) sample F9805-04 ($r^2 = 0.99$); (b) sample M9701-03d ($r^2 = 0.92$). Predicted values represent the DIC production calculated for each cell using the correct irradiance spectrum and the quantum yield determined for that experiment. One-to-one lines show where the calculated values would fall if they reproduced exactly the measured values for the same experiment. Error bars show the 95% confidence intervals for the measured DIC production values, calculated from the variability in replicate distilled water DIC measurements made over a 5-month period.

absorbance and irradiance, we multiplied each quantum yield spectrum by the same irradiance spectrum (that shown in Fig. 2 for the 295 nm cut-off filter). We summed over the wavelength range 280–480 nm to calculate a scaled "photochemical response" for each (Fig. 6). The largest photochemical response in Fig. 6 is about 21 times that of the smallest. One quantum yield spectrum clearly cannot be used to predict DIC production rate everywhere in the ocean.

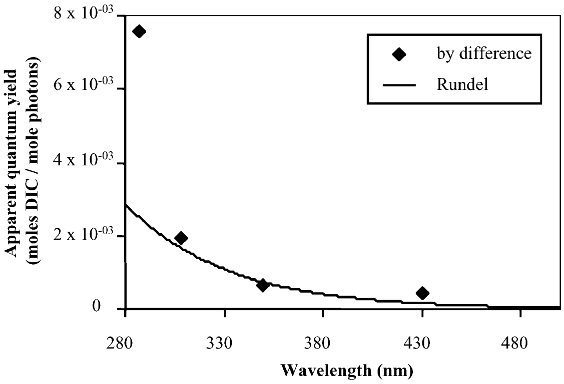

Fig. 5. Apparent quantum yield spectra for sample M9705-05, calculated using both the curve-fit and difference methods.

From this figure, we were able to distinguish three general groups of spectra. Since they grouped geographically, we used Fig. 6 to define the three geographic zones: inshore, including Halifax's turbid Bedford Basin, the North West Arm of Halifax Harbour, and surface samples just outside the Delaware Bay that were strongly terrestrially influ-

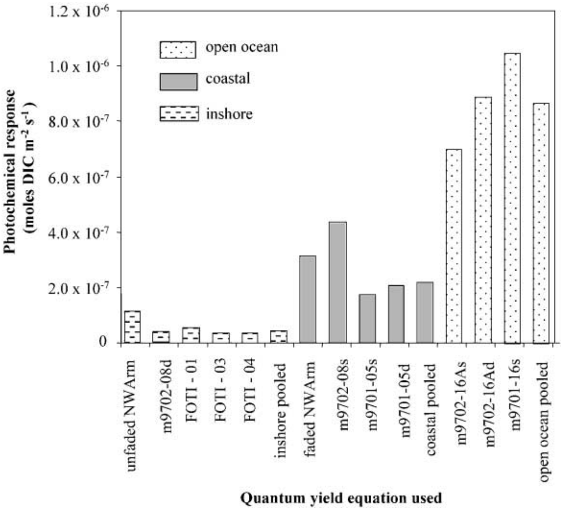

Fig. 6. "Photochemical response" calculated by multiplying each of the fourteen quantum yield spectra by an identical irradiance spectrum (the spectrum measured under the 295 nm cut-off filter in the solar simulator—see Fig. 2) and summing over the wavelength range 280–480 nm. These values should NOT be applied to the real ocean; they are included only to demonstrate the effect of the variability among quantum yield spectra on DIC production and the geographic grouping of spectra.

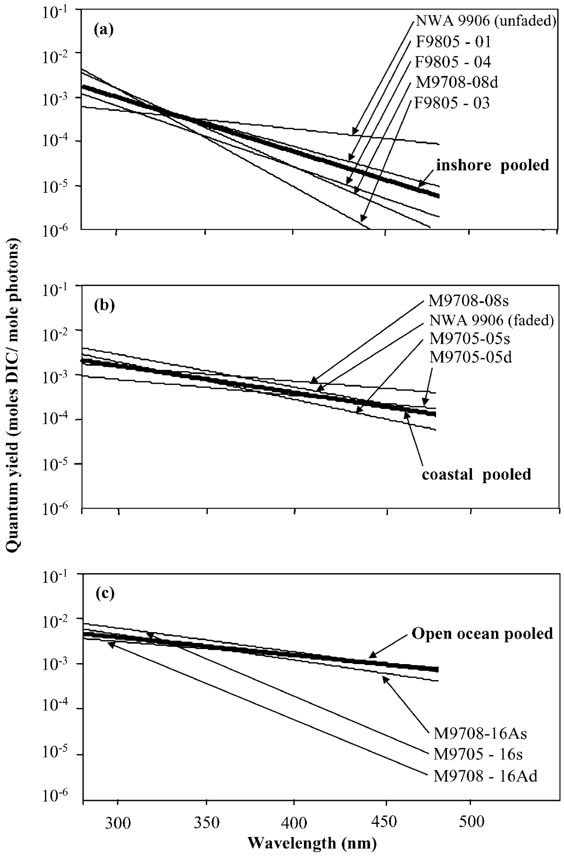

Fig. 7. Apparent quantum yield spectra for the photochemical production of DIC, arranged by zone, with zone-pooled spectra shown. (a) Inshore; (b) coastal; (c) open ocean.

enced; coastal, over the continental shelf in the Mid-Atlantic Bight; and open ocean, blue water samples taken from the Gulf Stream. (Fig. 6 was not used for any other purpose, and the scaled photochemical responses should not be taken to represent actual production rates in the ocean.) For the same irradiance spectrum, the inshore water is the least efficient at producing DIC, while the open ocean water is the most efficient. The quantum yield spectrum for the unfaded water from Halifax Harbour fit into the inshore category, while to judge from its calculated photochemical response, the prefaded sample was more like the coastal samples. The geographic zones corresponded to ranges in salinity: inshore samples had salinity less than 31, coastal from 31 to 35, and open ocean greater than 35 on the Practical Salinity Scale. The quantum yield spectra are plotted by zone in Fig. 7.

We calculated a pooled quantum yield spectrum for each zone by applying a single exponential fit to all the DIC production and irradiance data together for that zone. The equations of the pooled quantum yield spectra are recorded in Table 3, and Fig. 8 shows their 80% confidence intervals, which were determined from the confidence intervals around the iteratively determined equation coefficients, m_1 and m_2. Clearly, the confidence intervals for the three pooled spectra overlap. This is not surprising, however, considering the gradational boundaries between the environments represented. The fairly wide confidence intervals reflect the variability among the samples taken within each zone. The inshore and coastal zone spectra were more variable (r^2 of pooled spectra 0.83 and 0.82, respectively) than were those in the open ocean zone ($r^2 = 0.93$). (The confidence interval shown in Fig. 8 for the open ocean pooled spectrum is wider than are those for the other two zones in absolute value, but not as a proportion of the magnitude of the spectrum.) The pooled spectra showed trends of increasing magnitude and decreasing slope from inshore to offshore.

A finer scale trend apparent from the data was that the surface sample at any given station always had a steeper quantum yield slope than did the sample taken from below the surface mixed layer at the same station. This means that surface sample was

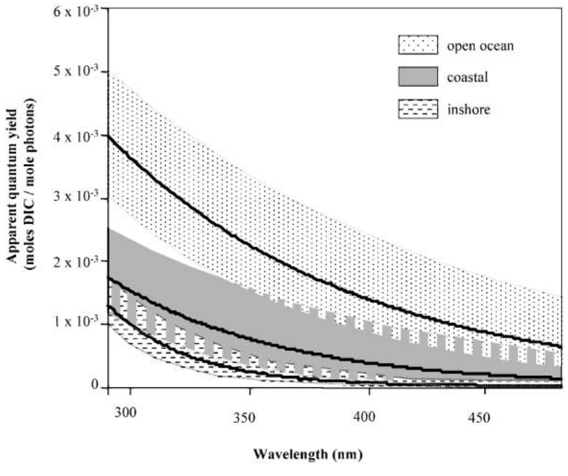

Fig. 8. Zone-pooled quantum yield spectra plotted with 80% confidence intervals calculated as described in text.

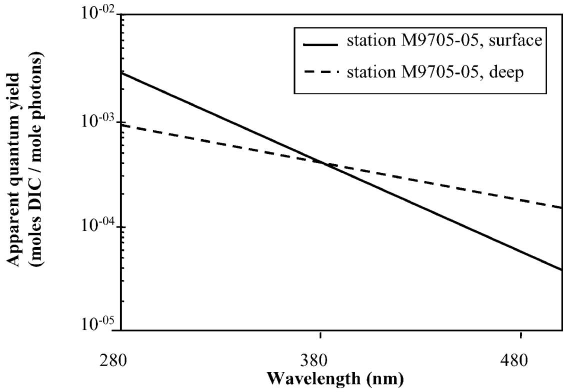

Fig. 9. Apparent quantum yield spectra for station M9705-05, showing the crossing of surface and deep spectra from the same station.

always more efficient in the UVB than was the deep sample. Corresponding pairs of surface and deep spectra crossed one another (Fig. 9, for example), although not at a consistent wavelength, so that the quantum yield values of the deep samples were higher than those of their surface counterparts in the visible region of the spectrum. It is not unreasonable that the water taken from two depths should show different photochemical characteristics; Vodacek et al. (1997), for example, reported a distinctly faded summer surface layer in the Mid-Atlantic Bight.

4. Discussion

Fig. 10 shows a comparison of the zone pooled quantum yield spectra determined in this study (and Johannessen, 2000) with those previously determined for lakes (Moore, 1999; Vähätalo et al., 2000a) and a river (Gao and Zepp, 1998). All the spectra were of similar magnitude. The lake spectra had steeper slopes than did the coastal and open ocean spectra, but they were slightly shallower than the inshore spectrum. Gao's and Zepp's river quantum yield points fell within a similar range, although the first point (at 290 nm) was higher than the other spectra at that wavelength.

Both the slope and the magnitude of the spectral quantum yield affect the production rate calculated from it. The zone pooled DIC quantum yield spectra presented here show greater magnitude and shallower spectral slope offshore than inshore. Fig. 6 shows that, as a result of the two geographic trends, the open ocean water samples produce DIC photochemically more efficiently than does either the coastal or the inshore water. The actual surface production rate depends on the colour of the water, and inshore water absorbs UV much more strongly than does open ocean water. Consequently, the relative importance of the three zones for carbon photochemistry in surface waters of the ocean is probably not so skewed toward the blue water as it appears from Fig. 6. However, if one considers photochemical production over the whole water column rather than surface production, then oligotrophic water does produce more DIC photochemically than does inshore water. Since CDOM is thought to be the main absorber of UV radiation in all areas of the ocean (Bricaud et al., 1981), UV will penetrate more deeply where there is a lower concentration of CDOM. Ultimately, for a particular irradiance field, about the same amount of UV radiation will be absorbed by CDOM over the whole water column, regardless of location. In that case, only the quantum yield, and not the colour of the water, will control whole water column DIC photoproduction.

The photochemical production of DIC in all areas of the ocean cannot be calculated accurately using a single quantum yield spectrum. However, it does seem possible to estimate DIC production regionally or locally, using a combination of three pooled spectra, for inshore, coastal, and open ocean water, with

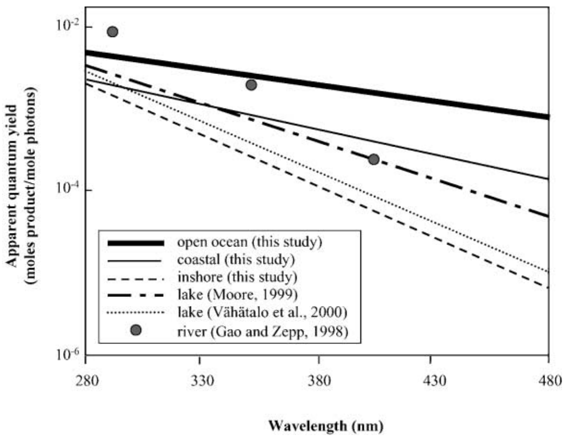

Fig. 10. Comparison of zone-pooled DIC quantum yield spectra determined in this study for marine water with quantum yield spectrum and points previously determined for fresh water.

appropriate absorptivity and irradiance spectra. More quantum yield determinations would be helpful in assessing the broad applicability of the pooled spectra presented here.

The inshore to offshore trend toward greater production efficiency suggests an insight into the DIC photoproduction mechanism. Considering terrestrially derived CDOM, one might expect that the more highly coloured, less degraded material found close to its source would produce DIC more efficiently than the molecules found offshore, but the opposite is true. The following explanation might resolve the apparent paradox.

Photodecarboxylation is the likely mechanism by which DIC is formed from CDOM (Chen et al., 1978). While the aromatic rings of synthetic lignin have been shown to produce DIC photochemically (Vähätalo et al., 2000b), suggesting that similar rings in CDOM do the same, in many molecules containing aromatic structures, it is the attached carboxylic acid functional groups, and not the ring structures themselves, that undergo photodecarboxylation to produce CO_2 (Budac and Wan, 1992). Inshore, terrestrially dominated CDOM contains more of the highly coloured, aromatic ring structures than does CDOM collected in the open ocean (Meyers-Schulte and Hedges, 1986), while both terrestrial and marine CDOM contain carboxyl groups (Libes, 1992). It is possible then, that the chiefly aromatic components of terrestrially derived CDOM contribute proportionally more to the absorbance of radiation than to DIC photoproduction. As the aromatic structures are eliminated by photochemical fading or as marine-derived CDOM begins to dominate absorbance, the proportion of DIC-producing to non-DIC-producing chromophores in CDOM increases. In this way, the efficiency of the dominant DIC-producing chromophores might remain constant, while the efficiency of the whole molecule for DIC production increased. The loss of non-DIC-forming chromophores by fading is supported by the increased quantum yield we determined in Halifax Harbour water after prolonged irradiation in the solar simulator. (However, that particular finding rests on a single experiment, which should be repeated for confirmation.) It is possible that other photochemical products might show different or even opposite trends in efficiency with location and irradiation history, depending on which components of CDOM produce them and on their relative roles in light absorption within the molecule.

5. Summary

In this paper, we have presented the first quantum yield spectra for DIC photoproduction in seawater. These spectra are essential for calculating the regional and global rates of DIC photoproduction. We have shown that, despite wide geographic variability in the spectral quantum yield of DIC, it is possible to represent quantum yield with three pooled spectra for geographic zones defined by salinity. We have also suggested a chemical interpretation of the trend toward increased efficiency of DIC photoproduction offshore. It should now be possible to combine optical data with these three spectra to make global estimates of DIC photoproduction in the ocean.

Acknowledgements

We thank Richard Davis, Rebecca Moore, Dr. Neil Blough, Jean-Paul Parkhill, Dr. Sherry Niven, Dr. Kumiko Azetsu-Scott, and the officers and crew of the *R/V Cape Henlopen* and the Coast Guard vessel *Ibis* for their assistance in collecting water samples and optical data. Dr. Aurea Ciotti, Dr. Huixiang Xie, Gary Maillet, Alex Feargrieve, Simon Trussler, and Jurgen Mueller gave us valuable assistance with the development of the laboratory methods and apparatus. We also thank Dr. John Cullen, Penny Kuhn, and Richard Davis for discussions about and assistance with the data analysis. We are grateful to five anonymous reviewers for their thoughtful comments. This research was funded by the Office of Naval Research (USA) and by the Natural Sciences and Engineering Research Council (Canada).

Associate editor: Dr. Paula Coble.

References

Andreae, M.O., Ferek, R.J., 1992. Photochemical production of carbonyl sulfide in seawater and its emission to the atmosphere. Global Biogeochem. Cycles 6, 175–183.

Balzani, V., Carassiti, V., 1970. Photochemistry of Coordination Compounds. Academic Press, London.

Blough, N.V., Zepp, R.G., 1995. Reactive oxygen species in natural waters. In: Foote, C.S., Valentine, J.S., Greenberg, A., Liebman, J.F. (Eds.), Active Oxygen in Chemistry. Chapman & Hall, New York, pp. 280–333.

Braslavsky, S.E., Houk, K.N., Verhoeven, J.W., 1996. Glossary of Terms Used in Photochemistry. 2nd edn. International Union of Pure and Applied Chemistry, Amsterdam.

Bricaud, A., Morel, A., Prieur, L., 1981. Absorption by dissolved organic matter of the sea (yellow substance) in the UV and visible domains. Limnol. Oceanogr. 26, 43–55.

Budac, D., Wan, P., 1992. Photodecarboxylation: mechanism and synthetic utility. Photochem. Photobiol. 67, 135–166.

Bushaw, K.L., Zepp, R.G., Tarr, M.A., Schulz-Jander, D., Boubonniere, R.A., Hodson, R.E., Miller, W.L., Bronk, D.A., Moran, M.A., 1996. Photochemical release of biologically labile nitrogen from dissolved organic matter. Nature 381, 400–404.

Chen, Y., Khan, S.U., Schnitzer, M., 1978. Ultraviolet irradiation of dilute fulvic acid solutions. Soil Sci. Soc. Am. J. 42, 292–296.

Cullen, J.J., Neale, P.J., 1994. Ultraviolet radiation, ozone depletion, and marine photosynthesis. Photosynth. Res. 39, 303–320.

Finden, D.A.S., Tipping, E., Jaworski, G.H.M., Reynolds, C.S., 1984. Light-induced reduction of natural iron (III) oxide and its relevance to phytoplankton. Nature 309, 783–784.

Gao, H., Zepp, R.G., 1998. Factors influencing photoreactions of dissolved organic matter in a coastal river of the southeastern United States. Environ. Sci. Technol. 32, 2940–2946.

Johannessen, S.C., 2000. A photochemical sink for dissolved organic carbon in the ocean. PhD thesis, Dalhousie University, Halifax, Canada.

Kieber, D.J., Mopper, K., 1987. Photochemical formation of glyoxylic and pyruvic acids in seawater. Mar. Chem. 21, 135–149.

Kieber, D.J., McDaniel, J., Mopper, K., 1989. Photochemical source of biological substrates in seawater: implications for carbon cycling. Nature 341, 637–639.

Kieber, R.J., Zhou, X., Mopper, K., 1990. Formation of carbonyl compounds from UV-induced photodegradation of humic substances in natural waters: fate of riverine carbon in the sea. Limnol. Oceanogr. 35, 1503–1515.

Libes, S.M., 1992. An Introduction to Marine Biogeochemistry. Wiley, Toronto.

Markager, S., Vincent, W.F., 2000. Spectral light attenuation and the absorption of UV and blue light in natural waters. Limnol. Oceanogr. 45, 642–650.

Meyers-Schulte, C.J., Hedges, J.I., 1986. Molecular evidence for a terrestrial component of humic matter dissolved in ocean water. Nature 321, 61–63.

Miller, W.L., 1994. Recent advances in the photochemistry of natural dissolved organic matter. In: Helz, G.R. (Ed.), Aquatic and Surface Photochemistry. Lewis Publishers, CRC Press, Boca Raton, pp. 111–128.

Miller, W.L., Kester, D.R., 1994a. Peroxide variations in the Sargasso Sea. Mar. Chem. 48, 17–29.

Miller, W.L., Kester, D.R., 1994b. Photochemical iron reduction and iron bioavailability in seawater. J. Mar. Res. 52, 325–343.

Miller, W.L., Moran, M.A., 1997. Interaction of photochemical and microbial processes in the degradation of refractory dissolved organic matter from a coastal marine environment. Limnol. Oceanogr. 42, 1317–1324.

Miller, W.L., Zepp, R.G., 1995. Photochemical production of dissolved inorganic carbon from terrestrial organic matter: significance to the oceanic organic carbon cycle. Geophys. Res. Lett. 22, 417–420.

Moore, R.J., 1999. Photochemical degradation of coloured dissolved organic matter in two Nova Scotian lakes. MSc thesis, Dalhousie University, Halifax, Canada.

Moore, C.A., Farmer, C.T., Zika, R.G., 1993. Influence of Orinoco River water on hydrogen peroxide distribution and production in the eastern Caribbean. J. Geophys. Res. 98, 2289–2298.

Mopper, K., Zhou, X., 1990. Hydroxyl radical photoproduction in the sea and its potential impact on marine processes. Science 250, 661–664.

Mopper, K., Zhou, X., Kieber, R.J., Kieber, D.J., Sikorski, R.J., Jones, R.D., 1991. Photochemical degradation of dissolved organic carbon and its impact on the oceanic carbon cycle. Nature 353, 60–62.

Moran, M.A., Zepp, R.G., 1997. Role of photochemistry in the formation of biologically labile compounds from dissolved organic matter. Limnol. Oceanogr. 42, 1307–1316.

Ratte, M., Bujok, O., Spitzy, A., Rudolph, J., 1998. Photochemical alkene formation in seawater from dissolved organic carbon: results from laboratory experiments. J. Geophys. Res. 103, 5707–5717.

Rundel, R.D., 1983. Action spectra and estimation of biologically effective UV radiation. Physiol. Plant. 58, 360–366.

Sikorski, R.J., Zika, R.G., 1993. Modeling mixed-layer photochemistry of H_2O_2: optical and chemical modeling of production. J. Geophys. Res. 98, 2315–2328.

Stedmon, C.A., Markager, S., Kaas, H., 2000. Optical properties and signatures of chromophoric dissolved organic matter (CDOM) in Danish coastal waters. Estuarine Coastal Shelf Sci. 51, 267–278.

Vähätalo, A.V., Salkinoja-Salonen, M., Taalas, P., Salonen, K., 2000a. Spectrum of quantum yield for photochemical mineralization of dissolved organic carbon in a humic lake. Limnol. Oceanogr. 45, 664–676.

Vähätalo, A.V., Salonen, K., Salkinoja-Salonen, M., Hatakka, A., 2000b. Photochemical mineralization of synthetic lignin in lake water indicates enhanced turnover of aromatic organic matter under solar radiation. Biodegradation 10, 415–420.

Valentine, R.L., Zepp, R.G., 1993. Formation of carbon monoxide from the photodegradation of terrestrial dissolved organic carbon in natural waters. Environ. Sci. Technol. 27, 409–412.

Vodacek, A., Blough, N.V., DeGrandpre, M.D., Peltzer, E.T., Nelson, R.K., 1997. Seasonal variation of CDOM and DOC in the Middle Atlantic Bight: terrestrial inputs and photooxidation. Limnol. Oceanogr. 42, 674–686.

Wetzel, R.G., Hatcher, P.G., Bianchi, T.S., 1995. Natural photolysis by ultraviolet irradiance of recalcitrant dissolved organic matter to simple substrates for rapid bacterial metabolism. Limnol. Oceanogr. 40, 1369–1380.

Xie, H., Moore, R.M., Miller, W.L., 1998. Photochemical production of carbon disulfide in seawater. J. Geophys. Res. C 103, 5331–5344.

Zafiriou, O.C., Dister, B., 1991. Photochemical free radical production rates: Gulf of Maine and Woods Hole—Miami transect. J. Geophys. Res. 96, 4939.

Zepp, R.G., Faust, B.C., Hoigné, J., 1992. Hydroxyl radical formation in aqueous reactions (pH 3–8) of iron (II) with hydrogen peroxide: the photo-Fenton reaction. Environ. Sci. Technol. 26, 313–319.

Zhou, X., Mopper, K., 1990. Determination of photochemically produced hydroxyl radicals in the sea and its potential impact on marine processes. Mar. Chem. 30, 71.